Bulgarian Chemical Communications, Volume 58, Issue 1 (pp. 44-51) 2026 *DOI: 10.34049/bcc.58.1.5725*

Unveil mechanism of action of parthenolide-9-one as an inhibitor for human erythroleukemia *via* molecular modeling, ADMET and MMGBSA analysis

H. D. Nguyen*

Faculty of Biology, Thai Nguyen University of Education, 24000, Thai Nguyen, Vietnam

Received: October 17, 2025; Revised: November 22, 2025

Leukemia poses a substantial global health challenge highlighting the demand for innovative therapies. Acute erythroid leukemia, an uncommon and aggressive variant of acute myeloid leukemia, presents difficulties owing to unfavorable prognosis and scarce treatment guidelines. Apoptosis emerges as a central therapeutic target in oncology, enabling targeted destruction of tumor cells and alleviating resistance. Caspase-3, a key effector enzyme, initiates apoptotic cascades by substrate cleavage, establishing it as an essential regulator in cancer. The present investigation assessed the molecular action of parthenolide-9-one as anti-erythroleukemic activity *via* inducing caspase-3 (3PD1) using *in silico* techniques. Molecular docking revealed parthenolide-9-one's superior affinity and orientation in the 3PD1 site compared to doxorubicin. Dynamic simulations over 100 ns confirmed enduring stability and uniform interactions. ADMET profiling indicated favorable pharmacokinetics for parthenolide-9-one, characterized by strong absorption and minimal metabolic engagement despite Ames toxicity. These observations position parthenolide-9-one as a viable candidate for erythroleukemic intervention *via* caspase-3-driven apoptosis, providing a basis for the development of refined derivatives that target apoptotic pathways in malignancy.

Keywords: Apoptosis, caspase-3, human erythroleukemia, molecular modeling, parthenolide-9-one.

INTRODUCTION

Leukemia is a specific type of hematological malignancy involving the abnormal proliferation of white blood cells, with 486,777 new cases and 305,033 deaths in 2022 [1]. Acute erythroid leukemia is a rare and aggressive subtype of acute myeloid leukemia which is often associated with poor prognosis and challenging treatment due to its rarity and lack of established protocols [2, 3]. Current chemotherapy employs agents to eradicate cancer cells by inhibiting their proliferation, while also damaging normal cells. Apoptosis constitutes a primary target in oncology, facilitating selective cell demise and resistance mitigation [4].

Computational-aided drug discovery involves techniques like virtual screening, molecular modeling, and property prediction to identify promising compounds [5]. This approach can help identify potential new drug candidates and optimize existing treatments for acute erythroid leukemia, potentially leading to improved patient outcomes and quality of life [6].

Plant-derived compounds have played a crucial role in the development of effective cancer treatments, with many current chemotherapy drugs originating from natural sources. These drugs target various cellular processes crucial for cancer cell growth and division [7]. Among these, a sesquiterpenoid named parthenolide-9-one exhibits diverse biological activities, including *in vitro* cytotoxicity, *in vivo* antitumor activity, and antiviral activity [8, 9]. Parthenolide-9-one also demonstrates cytotoxicity against the human erythroleukemic cell line (HEL cells) *via* inducing apoptosis in a dose- and time-dependent manner [10]. However, molecular mechanisms of parthenolide-9-one remain partially clarified, especially *via* computational methods such as molecular docking, dynamic simulations, and ADMET predictions. Thus, the present study aimed to investigate its anti-erythroleukemic activity through integrated computational tools to better understand the mechanism of action. These findings establish a foundation for empirical validation and refinement of parthenolide-9-one for effective erythroleukemia therapy.

MATERIALS AND METHODS

Materials

The structure of parthenolide-9-one (molecular formula of $C_{15}H_{18}O_4$ and molecular weight of 262.1205 *m/z)*, was collected from Pubchem database (https://pubchem.ncbi.nlm.nih.gov/). Doxorubicin, a chemotherapy drug approved for the treatment of various cancers, with a molecular formula of $C_{27}H_{29}NO_{11}$ and a molecular weight of

* To whom all correspondence should be sent:
E-mail: *hungnd@tnue.edu.vn*

543.1741 m/z, was chosen as the reference (Figure 1).

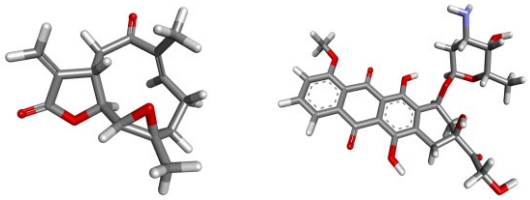

A B

Figure 1. 3D structures of parthenolide-9-one (A) and doxorubicin (B).

Evaluation of the biological activity of parthenolide-9-one

The evaluation of the biological activity of parthenolide-9-one against human erythroleukemic cell line (HEL cells) has been carried out in a previous study [10].

Molecular docking

Three-dimensional ligand structures were constructed in .pdb format using Biovia Discovery Studio Visualizer, retaining polar hydrogen atoms, calculating Gasteiger charges, and assigning full torsional flexibility. The three-dimensional structure of caspase-3 (PDB ID: 3PD1) was retrieved from the RCSB Protein Data Bank in .pdb format [11]. Molecular docking of protein and ligands employed AutoDock Tools, with grid dimensions set at x = 70, y = 52, z = 50, and spacing of 0.375 Å. Docking site coordinates were designated as x = 38.861 Å, y = 12.723 Å, z = 68.578 Å within the 3PD1 binding pocket. The Lamarckian genetic algorithm determined low-energy ligand-protein binding conformations.

Molecular dynamics simulation

Molecular dynamics simulations of the optimal docked conformation with caspase-3 (3PD1) were performed over 100 ns using GROMACS version 2024.4 [12]. The protein structure was refined with Swiss-PdbViewer to address missing atoms and residues [13]. Ligand topologies were derived using SwissParam [14]. A triclinic box with the SPC water model solvated the protein-ligand complex, incorporating 0.15 M sodium chloride. Structure optimization involved 50,000 energy minimization steps followed by 200 ps of NVT and 200 ps of NPT equilibration at 300 K and 1.0 bar. Trajectory data were recorded every 10 ns, and analyses of RMSD, RMSF, Rg, hydrogen bonds, and SASA were conducted using Grace software. Conformational stability comparisons were performed using UCSF Chimera 1.19 for superimposition [15].

Drug likeness and ADMET prediction

In silico studies, employing computational simulations, provide a standard method for assessing ADMET properties of drug candidates, aiding prediction of their *in vivo* behavior and informing drug discovery [16]. Consequently, the drug-likeness of selected iridoids was evaluated using pkCSM, a web server for predicting pharmacokinetic and toxicity profiles of small molecules [17].

Molecular mechanics generalized born surface area (MMGBSA) analysis

The MM/GBSA method, executed in gmx_MMPBSA with the charmm36-jul2022.ff force field, computed binding free energies for parthenolide-9-one–3PD1 and doxorubicin–3PD1 complexes. The generalized born model estimated electrostatic solvation energy in a continuum solvent, while non-polar solvation energy was derived from solvent-accessible surface area calculations. Analysis of molecular dynamics trajectories involved 125 snapshots extracted at 80 ps intervals over 80 ns (20–100 ns), providing an average binding energy that reflects dynamic protein-ligand interactions and reveals binding affinity and stability under simulated conditions.

RESULTS AND DISCUSSION

Docking analysis

Before ligand docking with 3PD1, active sites within the binding pocket were identified. Structural analysis of 3PD1 using Biovia Discovery Studio Visualizer revealed inhibition-related active sites (Fig. 2A).

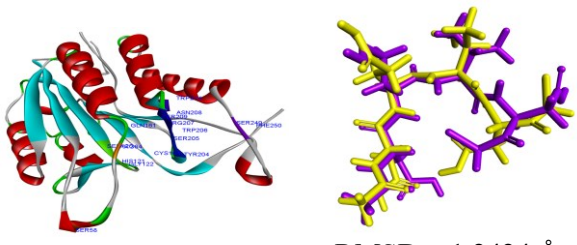

RMSD = 1.2424 Å

A B

Figure 2. Active sites within the 3PD1 protein (A) and superimposition of the docked and native ligands for validation of the molecular docking protocol (violet = native, yellow = docked) (B).

Redocking of the co-crystallized ligand confirmed the protocol's validity (Fig. 2B), with an RMSD of 1.2424 Å, and the ligand overlay verified accuracy. An RMSD below 2 Å validates the docking protocol's reliability [18]. The docked

complexes were evaluated based on their lowest binding energy values (kcal/mol). Table 1 summarizes the ligand interactions within the binding pockets of the 3PD1 protein. Figure 3 illustrates the interactions between the protein and ligands, including hydrogen bonds, van der Waals forces, and hydrophobic interactions.

Table 1. Interactions of docked ligands with the 3PD1 protein

N°	Docked ligands	Binding energy (kcal/mol)	Hydrogen bond interaction	Van der Waals interaction	Hydro-phobic interaction
1	Parthenolide-9-one	-7.81	Arg64, Gly122, Gln161, Arg207	Thr62, Ala162, Ser205	His121, Cys163, Tyr204
2	Doxorubicin	-6.31	Cys163, Arg207, Phe250, Asp253	Thr62, Ser205, Trp206, Asn208, Ser249, Ser251, Phe252, Phe256	His121, Arg207

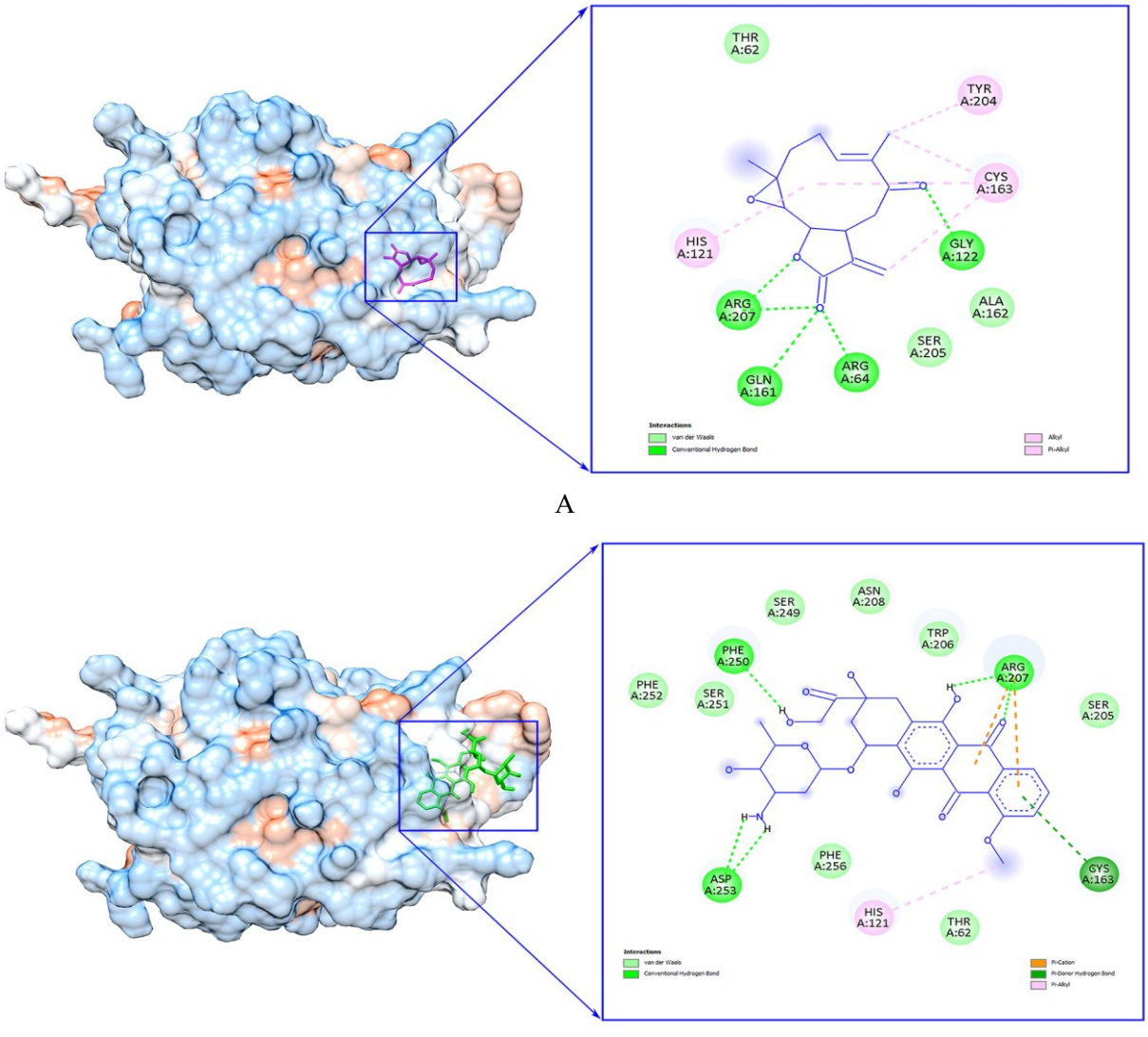

Figure 3. Molecular docking and two-dimensional interaction schematics for parthenolid-9-one (A) and doxorubicin (B) in complex with the 3PD1 protein.

Parthenolide-9-one exhibited interactions with the protein 3PD1 through four hydrogen bonds with amino acids Arg64, Gly122, Gln161, and Arg207, three van der Waals interactions with amino acids

Thr62, Ala162, and Ser205, and three hydrophobic interactions with amino acids His121, Cys163, and Tyr204. Among these, amino acids Arg64, His121, Gly122, Gln161, Cys163, Tyr204, Ser205, and Arg207 are located within the active sites of the protein 3PD1 (Fig. 3A). The binding energy for parthenolide-9-one with the protein 3PD1 was -7.81 kcal/mol.

Doxorubicin interacted with protein 3PD1 through four hydrogen bonds with amino acids Cys163, Arg207, Phe250, and Asp253, eight van der Waals interactions with Thr62, Ser205, Trp206, Asn208, Ser249, Ser251, Phe252, and Phe256, and two hydrophobic bonds with His121 and Arg207. Among these interactions, three amino acid residues, including His121, Ser205, Trp206, Arg207, Asn208, and Phe250, are placed within the active sites of the protein 3PD1. The binding energy for doxorubicin with the protein 3PD1 was -6.31 kcal/mol (Fig. 3B).

Parthenolide-9-one and doxorubicin were assessed for interactions with protein 3PD1, a target in apoptosis pathways relevant to human erythroleukemic cells. Both compounds formed hydrogen bonds, van der Waals, and hydrophobic interactions, contributing to ligand-protein complex stability [19]. Hydrogen bonds and hydrophobic contacts primarily drive binding specificity, while van der Waals interactions support structural integrity [20]. More negative binding energies correlate with stronger ligand-receptor affinity [21]. Parthenolide-9-one's superior binding energy and active-site interactions suggest enhanced potential for apoptosis induction in human erythroleukemic cells. Molecular dynamics simulations are recommended to further investigate parthenolide-9-one's dynamic behavior within 3PD1's binding pocket, using docked structures to compare with doxorubicin and validate its anti-cancer potential.

Molecular dynamics simulation

Molecular dynamics simulations, executed using GROMACS, were employed to analyze the binding behavior of the ligand-protein complex [22]. In this study, a molecular dynamics simulation analysis was carried out on the complexes parthenolide-9-one+3PD1 and doxorubicin+3PD1 to examine the RMSD, RMSF, Rg, H-bonds, and SASA. As a result, the total energy was calculated as -553,884 kcal/mol for parthenolide-9-one+3PD1 and -687,553 kcal/mol for doxorubicin+3PD1. The potential values were calculated as -554,504 kcal/mol for parthenolide-9-one+3PD1 and -688,276 kcal/mol for doxorubicin+3PD1. The system was equilibrated at a temperature of 300K.

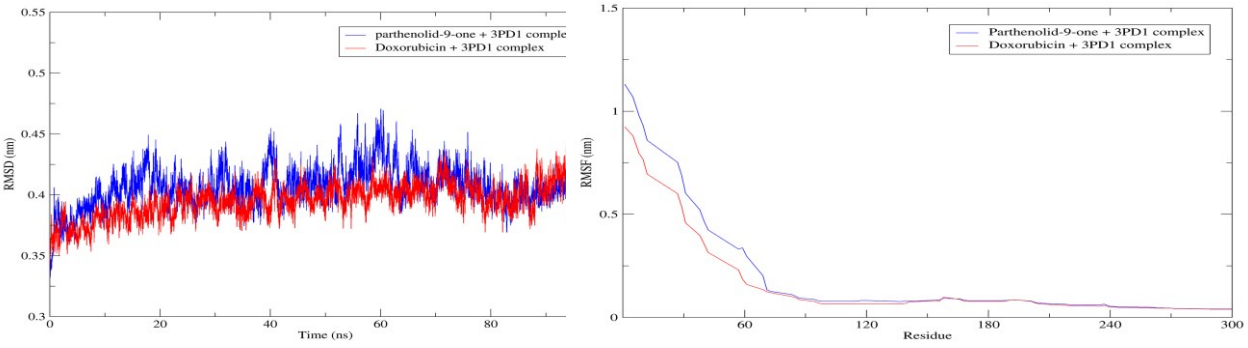

A B

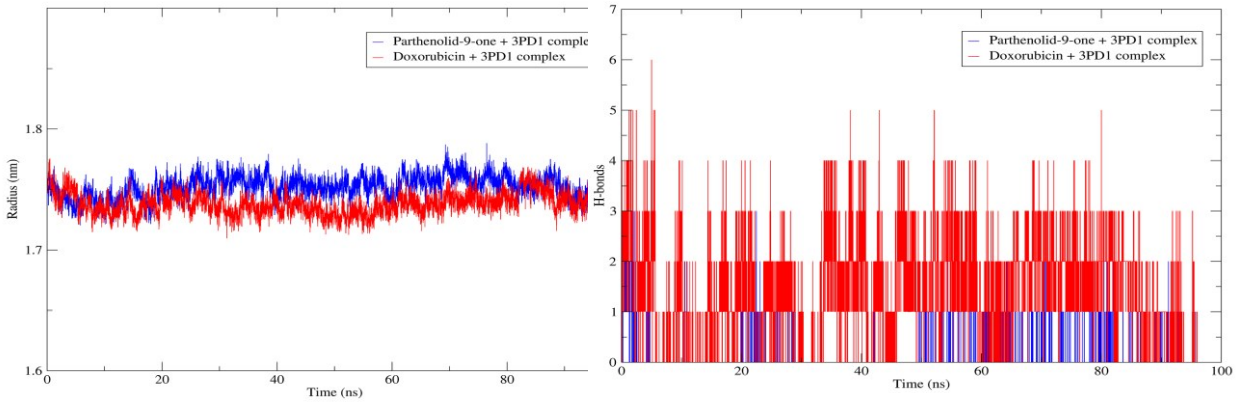

C D

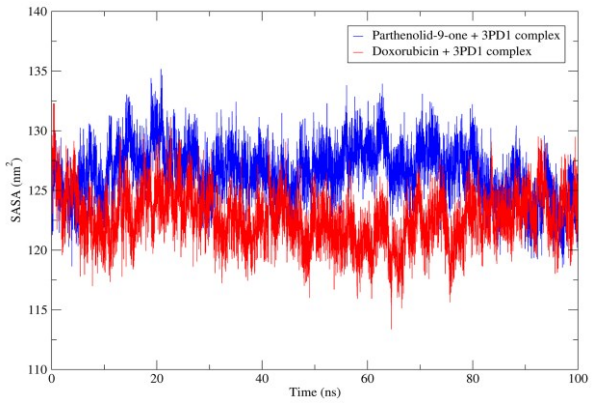

E

Figure 4. Results of MD simulation of parthenolide-9-one (blue) and doxorubicin (red) with 3PD1 protein. (A) RMSD, (B) RMSF, (C) Rg, (D) H-bonds, (E) SASA.

The RMSD values for the parthenolide-9-one+3PD1 and doxorubicin+3PD1 complexes ranged between 0.34 and 0.47 nm over a 100 ns simulation, with an average of approximately 0.42 nm throughout the simulation period (Fig. 4A). This result demonstrates that both parthenolide-9-one and doxorubicin sustained stable associations with protein 3PD1, exhibiting minor structural fluctuations indicative of equilibrated systems. The comparable average RMSD values for the parthenolide-9-one+3PD1 complex and the doxorubicin+3PD1 complex imply similar overall stability, consistent with the more negative docking binding energy of parthenolide-9-one (-7.81 kcal/mol) relative to doxorubicin (-6.31 kcal/mol).

Figure 4B illustrates the RMSF values for caspase-3 (3PD1), highlighting regions of structural flexibility that correspond to conformational variations. Conversely, residues in the active sites interacting with the ligands, including Arg64, His121, Gly122, Gln161, Cys163, Tyr204, Ser205, and Arg207 for parthenolide-9-one, and His121, Ser205, Trp206, Arg207, Asn208, and Phe250 for doxorubicin, display low RMSF values, denoting increased rigidity. The regions spanning residues 90–300, encompassing the binding pocket, exhibit diminished RMSF values for both complexes, underscoring pronounced structural stability and consistent ligand associations during the 100 ns simulation [23].

The Rg values for the complexes are presented in Figure 4C. The Rg values for both parthenolide-9-one9+3PD1 and doxorubicin+3PD1 complexes exhibited consistent stability, with an average fluctuation around 1.75 nm throughout the 100 ns simulation, signifying a compact conformation for caspase-3 (3PD1). This constancy suggests that ligand binding to the active sites of 3PD1, particularly involving residues 64–207, has a minimal influence on the protein's overall structure, thereby maintaining its conformational stability throughout the simulation duration [24].

Hydrogen bond counts in the parthenolide-9-one–3PD1 and doxorubicin–3PD1 complexes were measured to examine binding dynamics during simulation. Persistent bonds occurred throughout, with parthenolide-9-one ranging 1–4 and doxorubicin 1–6, denoting stable pocket interactions. Doxorubicin's broader range suggests higher variability, whereas parthenolide-9-one's narrower range indicates greater consistency over 100 ns, bolstering anticancer potential *via* superior docking energy (-7.81 *vs*. -6.31 kcal/mol) (Fig. 4D).

The SASA value was examined to assess solvent exposure levels in the 3PD1 complexes with parthenolide-9-one and doxorubicin. The SASA profiles exhibit oscillatory patterns in both complexes throughout the 100 ns simulation, with the parthenolide-9-one complex showing marginally reduced variability compared to the doxorubicin complex, suggesting ligand-induced alterations in solvent accessibility (Fig. 4E). These variations indicate structural adjustments at the 3PD1-ligand interface, which may affect binding affinity and stability, in agreement with parthenolide-9-one's superior docking binding energy of -7.81 kcal/mol relative to doxorubicin's -6.31 kcal/mol.

Supplementary evaluations using RMSD, RMSF, Rg, SASA, and hydrogen bond occupancy provided insights into the stability and dynamics of parthenolide-9-one–3PD1 and doxorubicin–3PD1 complexes. RMSD and RMSF revealed reduced fluctuations in parthenolide-9-one for overall stability and local flexibility. Rg assessments indicated equivalent protein compactness. SASA confirmed lower solvent exposure variability in parthenolide-9-one. Hydrogen bond analysis demonstrated a narrower, consistent range for

parthenolide-9-one. These parameters substantiate parthenolide-9-one's superior interactions with 3PD1, consistent with its binding energy (-7.81 *vs*. -6.31 kcal/mol). This stability enhances inhibition under physiological conditions and emphasizes anticancer potential in human erythroleukemic cells.

Drug likeness and ADMET prediction

ADMET evaluations were executed *via* the pkCSM platform to investigate the oral bioavailability of parthenolide-9-one and doxorubicin [25], with comprehensive findings detailed in Table 2.

Parthenolide-9-one showed human intestinal absorption of 98.971%, exceeding doxorubicin's 62.372%. Both express low absorption providing adequate gastrointestinal bioavailability, with parthenolide-9-one offering a notable advantage. Water solubility favored parthenolide-9-one at -2.674 log mol/L over doxorubicin's -2.915 log mol/L. $CaCO_2$ permeability was higher for parthenolide-9-one (1.278 log Papp in 10^{-6} cm/s) than for doxorubicin (0.457 log Papp in 10^{-6} cm/s), indicating superior membrane passage. Parthenolide-9-one evades P-glycoprotein substrate/inhibitor functions, thereby enhancing bioavailability by limiting efflux, unlike doxorubicin, which is a substrate without I/II inhibition, potentially hindering absorption and promoting resistance *in vivo*.

Distribution parameters for parthenolide-9-one revealed a restricted volume of distribution (VDss 0.037 log L/kg), contrasting with doxorubicin's wider distribution (1.647 log L/kg). Blood-brain barrier (BBB) thresholds define log BB >0.3 as favorable and <-1 as poor. Parthenolide-9-one's log BB of -0.055 indicates moderate permeability, while doxorubicin's -1.379 signifies limited crossing. Central nervous system (CNS) criteria categorize log PS > -2 as permeable and < -3 as impermeable. Parthenolide-9-one at -2.855 exhibits restricted CNS access, while doxorubicin at -4.307 shows inferior penetration. Fraction unbound (Fu) values of parthenolide-9-one at 0.492 *vs*. doxorubicin's 0.215, denote a greater free fraction for parthenolide-9-one to improve distribution, whereas doxorubicin's lower Fu suggests increased protein binding and bioavailability limitations.

Table 2. Predicted ADMET properties of parthenolide-9-one and doxorubicin

ADMET properties	Unit	Parthenolide-9-one	Doxorubicin
Water solubility	(Log mol/L)	-2.674	-2.915
$CaCO_2$ permeability	(Log Papp in 10-6 cm/s)	1.278	0.457
Intestinal absorption (Human)	(% Absorbed)	98.971	62.372
Skin permeability	(Log Kp)	-3.353	-2.735
P-glycoprotein substrate	Yes/No	No	Yes
P-glycoprotein I inhibitor	Yes/No	No	No
P-glycoprotein II inhibitor	Yes/No	No	No
VDss	(Log L/kg)	0.037	1.647
Fraction unbound (human)	(Fu)	0.492	0.215
BBB permeability	(Log BB)	-0.055	-1.379
CNS permeability	(Log PS)	-2.855	-4.307
CYP2D6 substrate	Yes/No	No	No
CYP3A4 substrate	Yes/No	No	No
CYP1A2 inhibitor	Yes/No	No	No
CYP2C19 inhibitor	Yes/No	No	No
CYP2C9 inhibitor	Yes/No	No	No
CYP2D6 inhibitor	Yes/No	No	No
CYP3A4 inhibitor	Yes/No	No	No
Total clearance	(Log ml/min/kg)	1.18	0.987
Renal OCT2 substrate	Yes/No	No	No
AMES toxicity	Yes/No	Yes	No
Max. tolerated dose (human)	(Log mg/kg/day)	0.27	0.081
hERG I inhibitor	Yes/No	No	No
hERG II inhibitor	Yes/No	No	Yes
Oral rat acute toxicity (LD50)	(mol/kg)	2.144	2.408
Oral rat chronic toxicity (LOAEL)	(Log mg/kg_bw/day)	2.216	3.339
Hepatotoxicity	Yes/No	No	Yes
Skin sensation	Yes/No	No	No
T. Pyriformis toxicity	(Log ug/L)	0.403	0.285
Minnow toxicity	(Log mM)	2.208	4.412

Table 3. Free energy of binding obtained using MMGBSA (kcal/mol).

N°	Parthenolide-9-one + 3PD1	Doxorubicin + 3PD1	N°	Parthenolide-9-one + 3PD1	Doxorubicin + 3PD1
ΔBOND	0.00	0.00	Δ1-4 VDW	-0.00	-0.00
ΔANGLE	0.00	-0.00	Δ1-4 E_{EL}	0.00	0.00
ΔDIHED	0.00	-0.00	ΔE_{GB}	8.65	27.11
ΔUB	0.00	0.00	ΔE_{SURF}	-1.37	-2.26
ΔIMP	-0.00	-0.00	ΔG_{GAS}	-13.36	-31.82
ΔCMAP	0.00	0.00	ΔG_{SOLV}	7.27	24.86
ΔVDWAALS	-9.71	-16.40	**ΔTOTAL**	**-6.08**	**-6.96**
ΔE_{EL}	-3.65	-15.41			

Parthenolide-9-one and doxorubicin present metabolic profiles that limit variability and interaction risks. Neither serves as a substrate for CYP2D6 or CYP3A4, nor inhibits CYP1A2, CYP2C19, CYP2C9, CYP2D6, or CYP3A4, reflecting negligible CYP450 engagement and low drug-drug interaction potential [26]. This non-reactive profile for parthenolide-9-one suggests stable metabolism, which bolsters therapeutic consistency. In contrast, doxorubicin's analogous traits align with its established application; however, oversight of alternative metabolic routes remains prudent for optimizing anticancer effects.

Excretion parameters were evaluated to outline clearance profiles of parthenolide-9-one and doxorubicin as potential therapeutics before removal. Predicted total clearance for parthenolide-9-one attained 1.18 log ml/min/kg, exceeding doxorubicin's 0.987 log ml/min/kg, denoting quicker systemic clearance for parthenolide-9-one. This variance, combined with neither as a renal OCT2 substrate, implies longer retention for doxorubicin, possibly permitting infrequent dosing. Higher clearance of parthenolide-9-one may necessitate frequent dosing for therapeutic maintenance, yet its -7.81 kcal/mol binding energy ensures robust target binding despite swift clearance.

Toxicity parameters were assessed to evaluate the safety profiles of parthenolide-9-one and doxorubicin. Parthenolide-9-one showed AMES toxicity, suggesting mutagenicity, unlike doxorubicin. Despite mutagenic concerns, parthenolide-9-one's strong 3PD1 binding (-7.81 kcal/mol) supports anticancer potential for erythroleukemic cells, warranting *in vivo* validation.

From the *in silico* ADMET evaluations of parthenolide-9-one and doxorubicin, the former manifests a viable pharmacokinetic profile despite AMES toxicity, characterized by superior absorption, moderate distribution, inert metabolism, and balanced clearance. Its robust binding to 3PD1 (-7.81 kcal/mol) underscores potential as a lead for anticancer treatment, targeting erythroleukemic cells *via* apoptosis. Parthenolide-9-one could underpin derivatives with refined safety, elevated efficacy, and novel apoptosis-directed mechanisms.

Free binding energy (MMGBSA) analysis

Binding free energies of the complexes were computed *via* the MM/GBSA approach in gmx_MMPBSA using the charmm36-jul2022.ff force field. Binding energy (ΔG_binding) equals G_complex - (G_receptor + G_ligand), or ΔH - TΔS, where effective free energy approximates without entropy for relative affinity comparisons. The effective binding energy was averaged from 125 snapshots taken at 80 ps intervals (20–100 ns) to capture the dynamic protein-ligand interactions under simulated conditions. MMGBSA values appear in Table 3. Effective free energies registered: -6.08 kcal/mol for parthenolide-9-one+3PD1 and -6.96 kcal/mol for doxorubicin+3PD1, indicate comparable affinities, with doxorubicin slightly more potent, aligning partially with docking trends favoring parthenolide-9-one.

CONCLUSIONS

The present study integrated molecular docking, dynamics simulations, and ADMET predictions to investigate parthenolide-9-one, focusing on its interaction with caspase-3 (3PD1). Docking results showed parthenolide-9-one's greater binding affinity and fit at the 3PD1 site *vs.* doxorubicin. 100 ns dynamics simulations verified stable parthenolide-9-

one–3PD1 binding, confirming reliable engagement with this apoptosis regulator. These findings endorse parthenolide-9-one as a caspase-3 modulator for apoptosis in erythroleukemic cells. Computational results necessitate experimental verification. Future work should prioritize laboratory assessments to fully examine parthenolide-9-one's interactions, including cellular impacts on efficacy and safety.

REFERENCES

1. F. Bray, M. Laversanne, H. Sung, J. Ferlay, R. L. Siegel, I. Soerjomataram, A. Jemal, *CA. Cancer J. Clin.*, **74**, 229 (2024).
2. P. Fernandes, N. Waldron, T. Chatzilygeroudi, N. S. Naji, T. Karantanos, *Int. J. Mol. Sci.*, **25**, 6256 (2024).
3. K. Gera, D. Martir, W. Xue, J. R. Wingard, *J. Clin. Oncol.*, **41**, e19031 (2023).
4. S. Elmore, *Toxicol. Pathol.*, **35**, 495 (2007).
5. S. K. Niazi, Z. Mariam, *Endocr. Diabetes Metab.*, **7**, e462 (2024).
6. S. Ghosh, S. Basu, T. Kayal, G. Ashok, S. Ramaiah, A. Anbarasu, *Discov. Appl. Sci.*, **7**, 491 (2025).
7. G. M. Cragg, D. J. Newman, *J. Ethnopharmacol.*, **100**, 72 (2005).
8. E. Abdel-Sattar, A. T. McPhail, *J. Nat. Prod.*, **63**, 1587 (2000).
9. [9] E. Abdel Sattar, A. M. Galal, G. S. Mossa, *J. Nat. Prod.*, **59**, 403 (1996).
10. S. Xu, Y. Tang, Y. Li, J. Yang, W. Gu, X. Hao, C. Yuan, *Bioorg. Chem.*, **139**, 106707 (2023).
11. J. Walters, P. Swartz, C. Mattos, A. C. Clark, *Arch. Biochem. Biophys.*, **508**, 31 (2011).
12. D. Van Der Spoel, E. Lindahl, B. Hess, G. Groenhof, A. E. Mark, H. J. C. Berendsen, *J. Comput. Chem.*, **26**, 1701 (2005).
13. N. Guex, M. C. Peitsch, *Electrophoresis*, **18**, 2714 (1997).
14. V. Zoete, M. A. Cuendet, A. Grosdidier, O. Michielin, *J. Comput. Chem.*, **32**, 2359 (2011).
15. E. F. Pettersen, T. D. Goddard, C. C. Huang, G. S. Couch, D. M. Greenblatt, E. C. Meng, T. E. Ferrin, *J. Comput. Chem.*, **25**, 1605 (2004).
16. L. Tao, P. Zhang, C. Qin, S. Y. Chen, C. Zhang, Z. Chen, F. Zhu, S. Y. Yang, Y. Q. Wei, Y. Z. Chen, *Adv. Drug Deliv. Rev.*, **86**, 83 (2015).
17. D. E. V Pires, T. L. Blundell, D. B. Ascher, *J. Med. Chem.*, **58**, 4066 (2015).
18. [M. J. Alves, H. J. C. Froufe, A. F. T. Costa, A. F. Santos, L. G. Oliveira, S. R. M. Osório, R. M. V Abreu, M. Pintado, I. C. F. R. Ferreira, *Molecules*, **19**, 1672 (2014).
19. R. Patil, S. Das, A. Stanley, L. Yadav, A. Sudhakar, A. K. Varma, *PLoS One*, **5**, e12029 (2010).
20. G. G. Ferenczy, M. Kellermayer, *Comput. Struct. Biotechnol. J.*, **20**, 1946 (2022).
21. S. Henrich, I. Feierberg, T. Wang, N. Blomberg, R. C. Wade, *Proteins Struct. Funct. Bioinforma.*, **78**, 135 (2010).
22. J. Martin, E. Frezza, *Front. Mol. Biosci.*, **9**, 970109 (2022).
23. C. Soremekun, D. Jjingo, D. Kateete, O. Nash, H. Grallert, A. Peters, T. Chikowore, C. Batini, O. Soremekun, S. Fatumo, *Next Res.*, **1**, 100041 (2024).
24. Z. K. Bagewadi, T. M. Yunus Khan, B. Gangadharappa, A. Kamalapurkar, S. Mohamed Shamsudeen, D. A. Yaraguppi, *Saudi J. Biol. Sci.*, **30**, 103753 (2023).
25. M. Zia, S. Parveen, N. Shafiq, M. Rashid, A. Farooq, M. Dauelbait, M. Shahab, A. M. Salamatullah, S. Brogi, M. Bourhia, *ACS Omega*, **9**, 2161 (2024).
26. F. P. Guengerich, Pharmacology and Toxicology of Cytochrome P450 – 60th Anniversary (Advances in Pharmacology, vol. 95), Academic Press, Boston, 2022.